Acta Mech. Sin. (2012) 28(1):146–150
DOI 10.1007/s10409-012-0018-6

RESEARCH PAPER

# Ultrasonic beam steering using Neumann boundary condition in multiplysics

**Zhao-Guo Qiu · Bin Wu · Cun-Fu He**

Received: 18 August 2010 / Revised: 26 February 2011 / Accepted: 21 March 2011


**Abstract** The traditional one-dimensional ultrasonic beam steering has time delay and is thus a complicated problem. A numerical model of ultrasonic beam steering using Neumann boundary condition in multiplysics is presented in the present paper. This model is based on the discrete wave number method that has been proved theoretically to satisfy the continuous conditions. The propagating angle of novel model is a function of the distance instead of the time domain. The propagating wave fronts at desired angles are simulated with the single line sources for plane wave. The result indicates that any beam angle can be steered by discrete line elements resources without any time delay.

**Keywords** Ultrasonic beam steering · Desired angle · Line element · Time delay

## 1 Introduction

Multilayered media such as bonded structures are increasingly used in industries due to their good mechanical properties. It is crucial to detect the defects that may appear either in the production process or in the entire service life of the structure. In bonded structures, interfacial weakness is one of the critical defects. Ultrasonic techniques are an important nondestructive evaluation tool for detecting adhesion weakness. Furthermore, the ultrasonic phased array and oblique incidence technique can improve the sensitivity of interface weakness detection without the necessity of utilizing a very high frequency.

Wave beam steering utilizing phased array and oblique incidence is a well-established technique and is applied extensively in ultrasonic imaging for medical and nondestructive evaluation [1,2]. Many studies have been carrying out for NDT application of beam steering utilizing phased array and oblique incidence. For example, Li et al. [3] implemented a phased comb transducer array using hardware and software delay and sum wave beam forming algorithms on pipes. Wilcox [4] presented a circular array integrated with a deconvolution algorithm to improve quality. Other researchers proposed the use of spatially distributed arrays, consisting of sensors distributed over a large area, as an effective approach to image damage inside and outside the area, enclosed by the array [5–11]. The method of application range from single element transducers to phased array elements for industrial inspection [12–19].

In many applications the incidence angle may be changed to steer the wavefront at the desired angle for broadening the range of the inspection. And the phased array is excited sequentially with a precomputed time-delay. Single-element transducers are mounted on wedges with known inclinations to obtain the desired angle of incidence in the specimen.

In this paper, by normal incidence the element line sources are applied to the simulation of a propagating wave front at a desired angle. And the beam is simulated by a number of discrete line elements which are excited without any time-delay. It is shown that the required beam steering angle is accurate in computation. The following sections present the beam steering using the Neumann boundary conditions and the essential criteria required in COMSOL.

## 2 Governing equations and analytical solution

The governing equation describes the induction of an acous-

The project was supported by the National Natural Science Foundation of China (10972014).

Z.-G. Qiu (✉) · B. Wu · C.-F. He
College of Mechanical Engineering
and Applied Electronics Technology,
Beijing University of Technology,
100124 Beijing, China
e-mail: hbsyjs@163.com

tic wave into the bonded structure. The wave equation is

$$\nabla\Big(\frac{1}{\rho}\nabla P\Big) = \frac{1}{\rho c^2}\frac{\partial^2 P}{\partial t^2}. \tag{1}$$

The form of Gaussian pulse window is excited as

$$P = -A\cos(\pi f t)\cdot \exp\Big[\frac{-4\pi(t-f/5)^2}{(f/4)^2}\Big], \tag{2}$$

where $P$ is the pressure (Pa), $\omega = 2\pi f$ is the angular frequency of the acoustic wave, $f$ is the frequency (Hz), $A$ is the amplitude, and $t$ is the time. The shear wave is used for solid, and longitudinal wave is used for fluid.

### 2.1 Boundary conditions

To model plane wave propagation, the line source whose length is governed by Neumann conditions is applied as ultrasonic transducer. The Gaussian pulse is adapted to generate time domain signal as shown in Fig. 1.

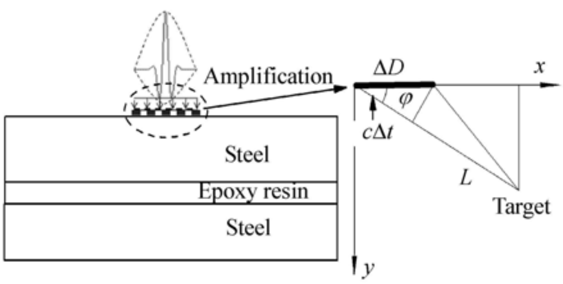


**Fig. 1** Principle of boundary condition excitation

The Neumann boundary condition is applied to $x$-axis, and Gauss pulse is applied to steer the ultrasonic transducer. The ultrasonic wave propagates along $y$-axis. Neumann boundary condition [20–22] is employed for the interface between the ultrasonic transducer and the steel. For time-harmonic displacement $\hat{u}(x,t) = \exp(-\mathrm{i}\omega t)u(x)$ with an angular frequency $\omega$ and imaginary unit $\mathrm{i} = \sqrt{-1}$, the time-harmonic waves in a domain $\Omega$ can be described by a Navier equation

$$-u'' = k^2 u \quad \text{in} \quad \Omega :\subset (0,1)\cdot R, \tag{3}$$

where $u'' = \partial^2 u/\partial x^2$, $u' = \partial u/\partial x$, $k = \omega/c$ is the consistency wave number, $c$ is wave velocity, $R$ is the transducer radius.

The boundary conditions is

$$-\mathrm{i}ku(0) - u'(0) = -2\mathrm{i}k, \quad -\mathrm{i}ku(1) - u'(1) = 0. \tag{4}$$

Let $[x_j]_{0\le j\le n}$ denote a set of gird points $0 \le x_0, x_1, \cdots, x_n \le 1$. The step size $h$ is defined by

$$h = \max_{1\le m\le n}(x_m - x_{m-1}). \tag{5}$$

It is easy to check that the exact solution of Eqs. (3) and (4) are given by

$$u(x) = \mathrm{e}^{\mathrm{i}kx}. \tag{6}$$

Similarly, the approximation solution of Eqs. (3)–(5) are given by

$$u(h)_m = \mathrm{e}^{\mathrm{i}k'h}, \quad m = 1, 2, \cdots, n, \tag{7}$$

where $k'$ is the discrete wave number.

The approximation of the exact solution of Eq. (3) is given as [23]

$$u(h) = \sum_{m=1}^{n} u_m\varphi_m(h), \tag{8}$$

where $\varphi_m$ are functions of nodal basis $h$, and $u(h)$ is approximation of the exact solution.

### 2.2 Relation of the consistency wave number to the discrete wave number

A generalized finite element method is applied to verify

$$k - k' = 0, \tag{9}$$

which is the relation of the consistency wave number to the discrete wave number.

The form of the generalized finite element method is

$$\boldsymbol{D}\boldsymbol{u} = \boldsymbol{b}, \tag{10}$$

where matrix $\boldsymbol{D}$ is

$$\boldsymbol{D} = \begin{bmatrix} D_1 & N & & & & \\ N & D_2 & N & & & \\ & N & D_3 & N & & \\ & & N & \ddots & \ddots & \\ & & & \ddots & D_n & N \\ & & & & N & D_1 \end{bmatrix}, \tag{11}$$

and a complex vector $\boldsymbol{u} = \{\boldsymbol{u}_q\}_{q\in Z=(1,2,\cdots,n+1)}$ vector $\boldsymbol{b}$ is

$$\boldsymbol{b} = [-2\mathrm{i}k \ \ 0 \ \ 0 \ \ 0 \ \ \cdots \ \ 0]^{\mathrm{T}}. \tag{12}$$

The element of $\boldsymbol{D}$ can be expanded into a Taylor series

$$\begin{aligned} D_1 &= \frac{1}{h}\Big\{1 - \mathrm{i}kh + \sum_{n=1}^{m}\alpha_n(kh)^{2n} \\ &\quad + \mathrm{i}kh\sum_{n=1}^{m}\beta_n(kh)^{2n} + O\Big[(kh)^{2(m+1)}\Big]\Big\}, \\ D_2 &= \frac{1}{h}\Big\{2 + \sum_{n=1}^{m}\gamma_n(kh)^{2n} + O\Big[(kh)^{2(m+1)}\Big]\Big\}, \\ N &= \frac{1}{h}\Big\{-1 + \sum_{n=1}^{m}\delta_n(kh)^{2n} + O\Big[(kh)^{2(m+1)}\Big]\Big\}, \\ D_3 &= D_4 = \cdots = D_n = D_2, \\ \alpha_1 + \beta_1 &= -\frac{1}{2}, \qquad \gamma_1 + 2\delta_1 = -1. \end{aligned} \tag{13}$$

Equation (10) can be solved explicitly based on the solution of Eq. (13) which can be solved by the discrete Fourier transform. The discrete Fourier transform of a complex vector is

$$\boldsymbol{u} = \{\boldsymbol{u}_p\}_{p\in z=(\cdots,-1,0,1,\cdots)}, \tag{14}$$

$$\hat{\boldsymbol{u}}(\xi) = F_{(\boldsymbol{u})}(\xi) = \sum_{p=-\infty}^{+\infty} \boldsymbol{u}_p \exp(-\mathrm{i}p\xi). \tag{15}$$

For a difference scheme with constant coefficients given by

$$(A\boldsymbol{u})_p = \sum_{l=-m}^{m} A_l u_{p+l}. \tag{16}$$

The difference operator corresponding to the generalized finite element method is given by

$$\mathrm{d}(k'h) = D_2 + 2N\cos(k'h), \tag{17}$$

where $k' = \frac{1}{h}\arccos(-D_2/2N)$.

The approximation solution is given by Eq. (18) (wave propagation in the positive direction)

$$u_j = C\exp(-\mathrm{i}k'j), \quad 2 \le j \le n-1. \tag{18}$$

The constant $C$ is determined by the boundary conditions

$$(\boldsymbol{Du})_1 = -2\mathrm{i}k, \qquad (\boldsymbol{Du})_0 = 0. \tag{19}$$

And $C$ is thus given by

$$C = [-k\mathrm{e}^{-\mathrm{i}k'}(D_1 + N\mathrm{e}^{\mathrm{i}k'h})]/\{D_1^2 \sin k' + 2D_1N\sin[k'(1-h)] + N^2\sin[k'(1-2h)]\}. \tag{20}$$

Together with Eq. (13), we get

$$\frac{D_2}{2N} = \left[2 + \sum_{n=0}^{\infty}\gamma_n(kh)^{2n}\right]\Big/\left\{2\left[-1 + \sum_{n=0}^{\infty}\delta_n(kh)^{2n}\right]\right\} = -\left[1 + \left(\delta_1 + \frac{1}{2}\gamma_1\right)(kh)^2 + \sum_{s=2}^{\infty}\zeta_s(kh)^{2s}\right]. \tag{21}$$

The discrete wave number is re-written to include wave number $k$

$$k' = \frac{1}{h}\arccos\left[1 + \left(\delta_1 + \frac{1}{2}\gamma_1\right)(kh)^2 + \sum_{s=2}^{\infty}\zeta_s(kh)^{2s}\right]. \tag{22}$$

Let $kh \to 0$, and $\cos(kh) \approx 1 - \frac{1}{2}(kh)^2$,

$$k' = \frac{1}{h}\left[\sqrt{-2\delta_1 - \gamma_1}kh + \sum_{s=1}^{+\infty}\rho_s'(kh)^{2s+1}\right]. \tag{23}$$

Using Eq. (13) one can re-written Eq. (23) as

$$k' = \frac{1}{h}\left[kh + \sum_{s=1}^{+\infty}\rho_s'(kh)^{2s+1}\right] = k + \sum_{s=1}^{+\infty}\rho_s'[k(kh)^{2s}], \tag{24}$$

$$k' - k = O[k(kh)^2], \tag{25}$$

where $O[k(kh)^2]$ is of higher order infinitesimal, and $s \ge 1$.

$$k' = k. \tag{26}$$

And thus we have demonstrated the relation of the consistency wave number to the discrete wave number. Equation (26) satisfies the usual continuous conditions.

Figure 1 captures the time-domain ultrasonic wave modeled with the Radiation boundary condition and a normal acceleration boundary condition, represented by the boundary condition, respectively.

$$\boldsymbol{n} \cdot \left(\frac{1}{\rho}\nabla P\right) + \frac{1}{c\rho}\frac{\partial P}{\partial t} = \boldsymbol{n} \cdot \frac{1}{\rho}\nabla P_i + \frac{1}{c\rho}\frac{\partial P_i}{\partial t}, \tag{27}$$

$$\boldsymbol{n} \cdot \left(\frac{1}{\rho}\nabla P\right) = a_n. \tag{28}$$

With $\boldsymbol{n}$ being the unit normal vector to the plane of the sides, $P_i$ is incident pressure wave; the steel-epoxy resin interface is Eq. (28).

We show the corresponding discretization of the transducer diameter. Using the results, we are able to construct an FEM with the property, and satisfying the usual continuous conditions.

## 3 Numerical simulations

The Helmholtz equation is solved using the finite element method. It is imperative that while solving by numerical technique, the node length $\Delta h$ should satisfy the following condition [24,25].

$$\frac{\Delta h}{\lambda} \le 1. \tag{29}$$

Or $k \cdot h$ = constant [24,25], $\lambda$ is the wavelength while $k$ is the magnitude of the wave vector, and it is equivalent to $\omega/c$.

Beam steering

Base on the foregoing formulation, the aim is to simulate practical cases in engineering applications. To validate the angle of incidence in bonded structures, the incidence angle is used to give the relation of reflection coefficient vs. degrees as shown in Fig. 2.

It is important to steer beam at desired angles. The interface between the steel and a layer of epoxy resin is assumed to be welded (ideal) or with interfacial debonding, respectively. The theoretical incidence angle for the steel-epoxy resin interface [26] is 32°. The reflection coefficient changes substantially when the incident angle has a slight perturbed deviation from 32°.

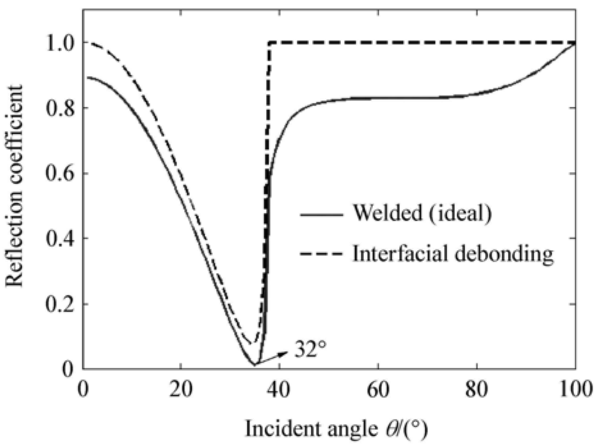


**Fig. 2** The reflection coefficients versus degrees for the steel-epoxyresin interfacial

All of the simulations were carried out for the steel plate, whose shear speed is 3 230 m/s and the density is 7 800 kg/m$^3$; the shear speed of epoxy resin is 1100m/s and the density is 1 300 kg/m$^3$. The thickness of bonded layer is 1 mm. The frequency of the wave under simulation was 1 MHz.

The other approach is based on the distance between the discrete line elements $\Delta D$ and time-delay $\Delta t$. Neumann boundary condition can be regarded as the slope of one direction. When Neumann boundary is used as the boundary condition for ultrasonic wave propagating, it can be regarded as partial differential of propagating in direction $L$.

$$\begin{aligned}\frac{d\Omega}{dL} = \frac{d\Omega}{dx}\cos(90^\circ - \theta_s) \Rightarrow \frac{d\Omega}{dL}\frac{dL}{d\Omega} &= \frac{d\Omega}{dx}\frac{dL}{d\Omega}\cos(90^\circ-\theta_s),\\ &\Rightarrow 1 = \frac{dL}{dx}\cos(90^\circ-\theta_s)\\ &\Rightarrow \cos(90^\circ-\theta_s) = \frac{dx}{dL}\\ &= \frac{\Delta D}{\Delta L} = \frac{c\Delta t}{\Delta D}\\ &\Rightarrow \cos(90^\circ-\theta_s) = \frac{c\Delta t}{\Delta D},\end{aligned}$$

$$\sin\theta_s = \frac{c\Delta t}{\Delta D}, \tag{30}$$

$$\cos(90^\circ-\theta_s) = \frac{c\Delta t}{\Delta D} = \frac{c(i\Delta t)}{n\Delta D}, \quad 1 < i < n, \tag{31}$$

where $c$ is the speed of wave in the steel medium, $D$ is the transducer diameter. From Eq. (31) it is clear that the incidence angle is governed by three parameters.

If we need to steer the beam at a desired angle, we need an estimation of time-delay $\Delta t$ to re-compute the discrete line elements $\Delta D$.

Let $c\Delta t = \Delta D$. $\Delta D$ is the discrete line elements, $\Delta t = \frac{1}{20f}$, so $\Delta D = \frac{c}{20f}$. Equation (31) is re-written to include an integer $n$, it is shown below in Eq. (32)

$$\cos(90^\circ-\theta_s) = \frac{i}{n}. \tag{32}$$

If $n$ represents integer greater than $i$, Eq. (32) can be used to create the desired angle. From Table 1 one can find some desired angle for shear wave. $\Delta D$ should be small so that the incidence angle will be steered with sufficient accuracy.

**Table 1** The different beam steering angles for shear wave

| $n$ | $i$ | $90^\circ - \theta_s/(^\circ)$ |
|---|---|---|
| 20 | 10 | 30 |
| 20 | 15 | 49 |
| 20 | 20 | 90 |

Results are presented for simulations using the above technique for three angles in the adhesive structures. Figure 3 denotes by solid lines the dominant energy orientations. We see that the beam steering technique implemented does simulate the desired angle. The angles in Fig. 3 are 30°, 49°, and 90°.

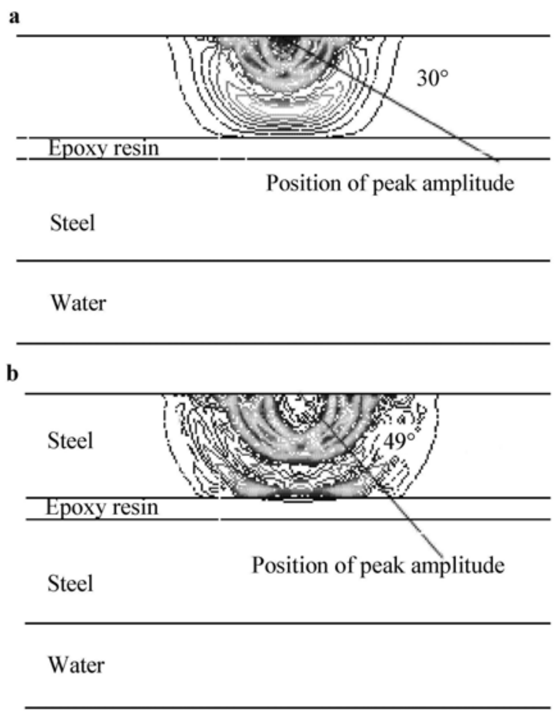


**Fig. 3** The different angles of beam steering in shear wave

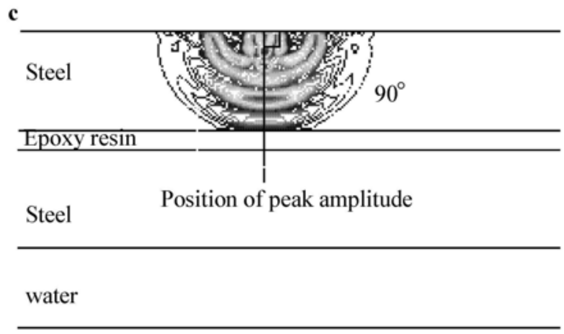


**Fig. 3** The different angles of beam steering in shear wave (continued)

## 4 Conclusions

(1) It is proved theoretically that the discrete wave number method can steer the beam angle, which satisfies the usual continuous conditions.
(2) With the FEM boundary condition, any beam angle rotation is simulated at normal incidence.
(3) By steering the numbers of discrete line sources for plane wave, the propagating wave fronts can be steered for desired beam angles without any time-delay.

## References


1 Achenbach, J.D.: Modeling for quantitative non-destructive evaluation. Ultrasonics **40**(1-8), 1–10 (2002)
2 Angel, Y.C., Achenbach, J.D.: Reflection and transmission of elastic waves by a periodic array of cracks: Oblique incidence. Wave Motion **7**(3), 375–397 (1985)
3 Li, J., Rose, J.L.: Implementing guided wave mode control by use of a phased transducer array. IEEE Trans. **48**, 761–768 (2001)
4 Wilcox, P.D.: Omni-directional guided wave transducer arrays for the rapid inspection of large areas of plate structures. IEEE Trans. **50**(6), 699–709 (2003)
5 Wang, C.H., Rose, J.T., Chang, F.K.: A synthetic time-reversal imaging method for structural health monitoring. Smart Mater. Struct. **13**(2), 415–423 (2004)
6 Michaels, J., Hall, J., Michaels, T.: A daptive imaging of damage from changes in guided wave signal recorded from spatially distributed arrays. Proc. SPIE **7395**(1), 1–15 (2009)
7 Roth, D.J., Tokars, R.P.: Ultrasonic phased array inspection for an isogrid structural element with cracks. NASA/TM, 1–19 (2010)
8 Deng, F.Q., Zhang, B.X., Wang, D.: Radiation acoustic field of a linear phased array on a cylindrical surface. Chin. Phys. Lett. **23**(12), 3297–3300 (2006)
9 Ozeri,S., Shmilovitz, D., Singer, Sigmond.: Ultrasonic transcutaneous energy transfer using a continuous wave 650 kHz Gaussian shaded transmitter. Ultrasonics **50**(7), 666–674 (2010)
10 Wooh, S.C., Shi, Y.J.: Optimum beam steering of linear phased arrays. Wave Motion **29**(3), 245–265 (1999)
11 Azar, L., Shi, Y., Wooh, S.C.: Beam focusing behavior of linear phased arrays. NDT & E International **33**(3), 189–198 (2000)
12 Elfgard, K.: Curved arrays for pipe wall inspection-fundamentals of electronic focusing for curved and plane arrays. Wave Motion **46**(4), 221–236 (2009)
13 Kono, N.Y., Nakahata, K.Y.: Modeing of phased array transducer and simulation of flow echoes. Science Links Japan **73**(10), 88–95 (2007)
14 Kimoto, K., Ueno, S., Hirose, S.: Image-based sizing of surface-breaking cracks by SH-wave array ultrasonic testing. Ultrasonics **45**(1-4), 152–164 (2006)
15 Mcnab, A., Capbell, M.J.: Ultrasonic phsaed arrays for nondestructive testing. NDT Int. **20**(6), 333–337 (2007)
16 Yu, L., Giurgiutiu, V.: In situ 2-D piezoelectric wafer active sensors arrays for guided wave damage detection. Ultrasonics **48**(2), 117–134 (2008)
17 Kim, D., Philen, M.: On the beamsteering characteristics of MFC phased arrays for structural health monitoring. In: Proc. of 49th AIAA/ ASME Structures, 1–6 (2008)
18 Liu, W., Hong, J.W.: Three-dimensional Lamb wave propagation excited by a phased piezoelectric array. Smart Mater **19**(8), 1–12 (2010)
19 Kim, D., Philen, M.: Guided wave beamsteering using MFC phased arrays for structural health monitoring. Journal of Intelligent Material Systems and Structures **21**(2), 1011–1024 (2010)
20 Friedlander, L.: Some inequalities between Dirichlet and Numann eigenvalues. Arch Rational Mech. Anal. **116**(2), 153–160 (1991)
21 Driscoll, T., Gottlieb, H.P.W.: Isospectral shapes with Neumann and alternating boundary condition. Phys. Rev. E **68**(1), 016702–016702 (2003)
22 Jakobson, D., Levitin, M., Nadirashvili, N.: Spectral problems with mixed Dirichlet-Neumann boundary condition. Journal of Computational and Applied Mathematics **194**(1), 141–155 (2006)
23 Parzanchevski, O., Ram, B.: Linear representations and isospectrality with boundary conditions. Journal of Geometric Analysis **20**(2), 439–471 (2010)
24 Raman, V., Abbas, A., Sunil, C.K.J.: Mapping local cavitation events in high intensity ultrasound fields. Excerpt from the Proceeding of the COMSOL Users Conference, Bangalore, 1–6 (2006)
25 Castaings, M., Predoi, M.V., Hosten, B.: Ultrasound propagation in viscoslastic material guides. In: Proceedings of the COMSOL Users Conference, Paris, 1–6 (2005)
26 Pilarski, A., Rose, J.L., Balasubramaniam, K.: The angular and frequency characteristics of reflectivity from a solid layer embedded between two solids with imperfect boundary conditions. J. Acoust. Soc. Am. **87**(2), 532–541 (1990)